ISSN 1674-1056
http://cpb.iphy.ac.cn
http://iopscience.iop.org/cpb
中国物理 B
Chinese Physics
中国物理 Chinese Physics B

Theoretical analytic model for RESURF AlGaN/GaN HEMTs

Hao Wu(吴浩), Bao-Xing Duan(段宝兴), Luo-Yun Yang(杨珞云), Yin-Tang Yang(杨银堂)

Citation: Chin. Phys. B . 2019, 28(2): 027302. **doi:** 10.1088/1674-1056/28/2/027302
Journal homepage: http://cpb.iphy.ac.cn; http://iopscience.iop.org/cpb

What follows is a list of articles you may be interested in

1.8-kV circular AlGaN/GaN/AlGaN double-heterostructure high electron mobility transistor

Sheng-Lei Zhao(赵胜雷), Zhi-Zhe Wang(王之哲), Da-Zheng Chen(陈大正), Mao-Jun Wang(王茂俊), Yang Dai(戴扬), Xiao-Hua Ma(马晓华), Jin-Cheng Zhang(张进成), Yue Hao(郝跃)

Chin. Phys. B . 2019, 28(2): 027301. **doi:** 10.1088/1674-1056/28/2/027301

Low specific on-resistance GaN-based vertical heterostructure field effect transistors with nonuniform doping superjunctions

Wei Mao(毛维), Hai-Yong Wang(王海永), Peng-Hao Shi(石朋毫), Xiao-Fei Wang(王晓飞), Ming Du(杜鸣), Xue-Feng Zheng(郑雪峰), Chong Wang(王冲), Xiao-Hua Ma(马晓华), Jin-Cheng Zhang(张进成), Yue Hao(郝跃)

Chin. Phys. B . 2018, 27(4): 047305. **doi:** 10.1088/1674-1056/27/4/047305

Simulation study of InAlN/GaN high-electron mobility transistor with AlInN back barrier

Tie-Cheng Han(韩铁成), Hong-Dong Zhao(赵红东), Lei Yang(杨磊), Yang Wang(王杨)

Chin. Phys. B . 2017, 26(10): 107301. **doi:** 10.1088/1674-1056/26/10/107301

A novel enhancement mode AlGaN/GaN high electron mobility transistor with split floating gates

Hui Wang(王辉), Ning Wang(王宁), Ling-Li Jiang(蒋苓利), Xin-Peng Lin(林新鹏), Hai-Yue Zhao(赵海月), Hong-Yu Yu(于洪宇)

Chin. Phys. B . 2017, 26(4): 047305. **doi:** 10.1088/1674-1056/26/4/047305

Fabrication and characterization of V-gate AlGaN/GaN high electron mobility transistors

Zhang Kai, Cao Meng-Yi, Chen Yong-He, Yang Li-Yuan, Wang Chong, Ma Xiao-Hua, Hao Yue

Chin. Phys. B . 2013, 22(5): 057304. **doi:** 10.1088/1674-1056/22/5/057304

Theoretical analytic model for RESURF AlGaN/GaN HEMTs*

Hao Wu(吴浩)†, Bao-Xing Duan(段宝兴)‡, Luo-Yun Yang(杨珞云), and Yin-Tang Yang(杨银堂)

Key Laboratory of the Ministry of Education for Wide Band-Gap Semiconductor Materials and Devices, Xidian University, Xi'an 710071, *China*

(Received 26 October 2018; revised manuscript received 3 December 2018; published online 10 January 2019)

In this paper, we propose a two-dimensional (2D) analytic model for the channel potential and electric field distribution of the RESURF AlGaN/GaN high electron mobility transistors (HEMTs). The model is constructed by two-dimensional Poisson's equation with appropriate boundary conditions. In the RESURF AlGaN/GaN HEMTs, we utilize the RESURF effect generated by doped negative charge in the AlGaN layer and introduce new electric field peaks in the device channels, thus, homogenizing the distribution of electric field in channel and improving the breakdown voltage of the device. In order to reveal the influence of doped negative charge on the electric field distribution, we demonstrate in detail the influences of the charge doping density and doping position on the potential and electric field distribution of the RESURF AlGaN/GaN HEMTs with double low density drain (LDD). The validity of the model is verified by comparing the results obtained from the analytical model with the simulation results from the ISE software. This analysis method gives a physical insight into the mechanism of the AlGaN/GaN HEMTs and provides reference to modeling other AlGaN/GaN HEMTs device.

Keywords: RESURF AlGaN/GaN HEMTs, two-dimensional analytic model, potential distribution, electric field distribution

PACS: 73.40.Kp, 85.30.Tv, 85.30.De **DOI:** 10.1088/1674-1056/28/2/027302

1. Introduction

The electronic properties of GaN material such as wide bandgap, high breakdown electronic field and high electron saturation velocity make it possess a very popular application in high-power and high-frequency power devices.[1,2] In recent years, the AlGaN/GaN high electron mobility transistors (HEMT)s have drawn much attention from researchers due to high-density two-dimensional electron gas (2DEG), which is observed at AlGaN/GaN heterojunction interfaces with strong polarization effects. The characteristic of high conductivity and high mobility for 2DEG, enables AlGaN/GaN HEMT to possess excellent microwave power performance.[3–5] The breakdown voltage (BV) is a significant parameter to evaluate a certain power handling capability for the power device. To improve the BV of the device, many different methods have been proposed, such as the field plate HEMTs, the low density drain HEMTs, ion implantation technique, the RESURF HEMTs, *etc*. Here, we mainly focus on the RESURF technology. The concept of RESURF technology originates from silicon-based semiconductor devices and it has been widely used in GaN-based HEMTs.[6–8]

So far, all the structures mentioned above have been fabricated or numerically simulated. However, the mechanism of breakdown voltage reduction has not been revealed. It is known that the numerical analytical method is an effective way to gain a physical insight into the breakdown characteristic of the device. Mao *et al.* proposed an analytical model for the off-state channel electric field distribution of field-plated AlGaN/GaN HEMTs.[9] Kumar *et al.* established an analytical model for the dual-material-gate AlGaN/GaN HEMTs. This analytical model accurately predicts the channel potential and electric field only for small geometry devices under low bias voltages.[10] To our knowledge, no analytical model is developed to investigate the potential and electronic field distribution of AlGaN/GaN HEMTs with high drain–source voltage. Therefore, it is necessary to build an analytical model for it.

In this work, we aim to analyze the structure proposed by Duan and Yang,[7] the RESURF AlGaN/GaN HEMTs. In contrast to traditional AlGaN/GaN HEMTs, the electric field of RESURF AlGaN/GaN HEMTs below the gate edge is reduced and new electronic field peaks arise. These phenomena result from the electronic field modulation effect that the added negative charge assists the depletion of 2DEG. The analytical model for the potential and electric field distribution is obtained by solving the 2D Poisson's equation with appropriate boundary conditions and approximation. The dependence of the channel potential and electric field distribution on the charge doping position and doping density in the AlGaN layer are discussed in detail. The analytical results of the model proposed fit well with the simulation results. We obtain our simulation results by the ISE TCAD software. The analytical approach given in this paper can also be applied to modeling other HEMTs, and guide the device engineers in designing and optimizing the HEMTs device.

*Project supported by the National Basic Research Program of China (Grant No. 2015CB351906), the National Natural Science Foundation of China (Grant No. 61774114), the Key Program of the National Natural Science Foundation of China (Grant No. 61334002), and the 111 Project, China (Grant No. B12026).

†Corresponding author. E-mail: haowu1701@163.com

‡Corresponding author. E-mail: bxduan@163.com

© 2019 Chinese Physical Society and IOP Publishing Ltd

2. Model of RESURF AlGaN/GaN HEMTs

Figure 1 shows the schematic cross-section of the RESURF AlGaN/GaN HEMT with a double LDD. The epitaxial structure consists of a substrate layer, an AlN nucleation layer, and then a heterojunction which is composed of a GaN buffer layer and an AlGaN barrier layer. For the RESURF AlGaN/GaN HEMT, negative charge is introduced to the surface of the AlGaN/GaN heterojunction in the AlGaN layer by ion implantation.

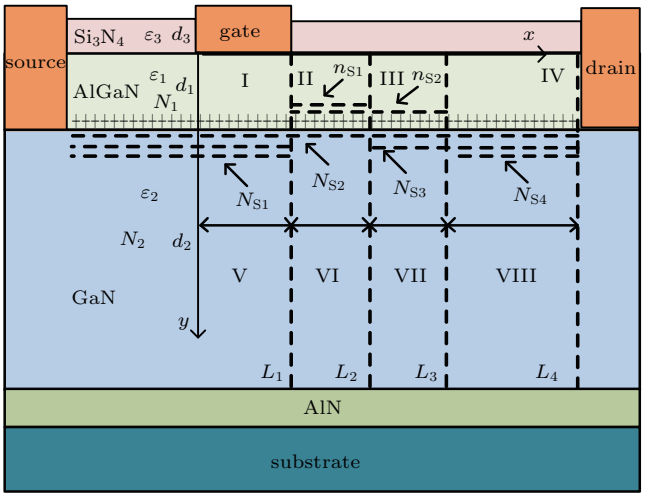


Fig. 1. Cross-section of RESURF AlGaN/GaN HEMTs with double LDD.

The negative charge added in the RESURF AlGaN/GaN HEMTs can help to deplete the 2DEG in the channel of the device, and it is an electric field modulation generated by the added positive charge.[11] Furthermore, in order to effectively improve the BV of the device, the charge density in the region near the gate edge needs to be larger than in another region.

As shown in Fig. 1, all the important parameters are given. Here x represents the horizontal distance from the gate edge near the source and y measures the vertical distance from the surface of the AlGaN barrier layer. In this paper, the epitaxial structure consists of a 0.5-nm Si_3N_4 passivation layer, 25-nm AlGaN barrier layer, and a 4-μ m-thick GaN buffer layer. We express the thickness of AlGaN, GaN and Si_3N_4 with d_1, d_2, and d_3 respectively. In this paper, m is used to express the molar fraction of Al in the AlGaN barrier, which equals 0.25. The source length, the drain length, the gate length, and the gate-to-drain spacing are 0.5 μm, 0.5 μm, 1.5 μm, and 5 μm, respectively. The ε_1, ε_2, and ε_3 denote the dielectric constant of AlGaN layer, Si_3N_4 passivation layer, and GaN buffer layer, respectively. The L_1 represents the length of the gate; L_2–L_1 denotes the length of the doping region near the gate in the AlGaN layer; L_3–L_2 is the length of the doping region on the drain side; L_4 indicates the distance from the gate edge near the source to the drain edge near the gate. For convenience, we denote L_2–L_1 and L_3–L_2 as l_1 and l_2 respectively in the following discussion. The N_1 and N_2 are the concentrations of acceptor carriers in the AlGaN barrier layer and the GaN buffer layer, respectively; N_{S1}, N_{S2}, N_{S3}, and N_{S4} denote the areal densities of 2DEG in different regions of the AlGaN/GaN heterojunction interface; n_{S1} and n_{S2} represent the negative charge doping densities in different doping regions. The source electrode of the device is grounded. The V_{DS} and V_{GS} are the bias voltage of the drain and gate, respectively.

We simulate the structure depicted in Fig. 1 by using the TCAD software. The generated results show that the area between the gate and the source is depleted very little. Thus, this part is neglected in the following discussion. We focus our attention on the region between the gate and the drain, where the electric field peaks of the device are located. According to the different structural parameters of the device, we divide the device into eight parts, which are denoted as I, II, III, IV, V, VI, VII, VIII. The boundaries of the eight regions are located at $x = 0, L_1, L_2, L_3, L_4$, $y = 0, d_1, d_1 + d_2$, respectively.

The potential distribution function of each part is expressed as $\varphi_i(x,y)$, i = 1–8, which satisfies the following 2D Poisson's equation:

$$\frac{\partial^2\varphi_i(x,y)}{\partial x^2}+\frac{\partial^2\varphi_i(x,y)}{\partial y^2}=-\frac{qN_1}{\varepsilon_1},\quad i=1,2,3,4, \tag{1}$$

$$\frac{\partial^2\varphi_i(x,y)}{\partial x^2}+\frac{\partial^2\varphi_i(x,y)}{\partial y^2}=-\frac{qN_2}{\varepsilon_2},\quad i=5,6,7,8. \tag{2}$$

The boundary conditions for Eqs. (1) and (2) are as follows.

According to the continuity of the electric displacement at the Si_3N_4 passivation layer and the AlGaN barrier layer interface, we can obtain

$$\varepsilon_1\frac{\partial\varphi_2(x,y)}{\partial y}\bigg|_{y=0}=\varepsilon_3\frac{\varphi_2(x,0)-V_p(x)}{d_3}, \tag{3}$$

$$\varepsilon_1\frac{\partial\varphi_3(x,y)}{\partial y}\bigg|_{y=0}=\varepsilon_3\frac{\varphi_3(x,0)-V_p(x)}{d_3}, \tag{4}$$

$$\varepsilon_1\frac{\partial\varphi_4(x,y)}{\partial y}\bigg|_{y=0}=\varepsilon_3\frac{\varphi_4(x,0)-V_p(x)}{d_3}, \tag{5}$$

where $V_p(x)$ represents the surface potential between the Si_3N_4 passivation layer and the air contact surface, which can be obtained by numerical fitting and is expressed as a parabolic function as follows:

$$V_p(x)=a_0x^2+a_1x+a_2. \tag{6}$$

Electric displacement continuity at the interface between the AlGaN layer and the GaN layer is shown below.

$$\varepsilon_1\frac{\partial\varphi_1(x,y)}{\partial y}\bigg|_{y=d_1}-\varepsilon_2\frac{\partial\varphi_5(x,y)}{\partial y}\bigg|_{y=d_1}=qN_{S1}, \tag{7}$$

$$\varepsilon_1\frac{\partial\varphi_2(x,y)}{\partial y}\bigg|_{y=d_1}-\varepsilon_2\frac{\partial\varphi_6(x,y)}{\partial y}\bigg|_{y=d_1}=qN_{S2}, \tag{8}$$

$$\varepsilon_1 \left.\frac{\partial \varphi_3(x,y)}{\partial y}\right|_{y=d_1} - \varepsilon_2 \left.\frac{\partial \varphi_7(x,y)}{\partial y}\right|_{y=d_1} = qN_{S3}, \quad (9)$$

$$\varepsilon_1 \left.\frac{\partial \varphi_4(x,y)}{\partial y}\right|_{y=d_1} - \varepsilon_2 \left.\frac{\partial \varphi_8(x,y)}{\partial y}\right|_{y=d_1} = qN_{S4}. \quad (10)$$

With $N_{S2} = N_{S1} - n_{S1}$, $N_{S3} = N_{S1} - n_{S2}$, $N_{S4} = N_{S1}$. This is due to the effect of negative charge on the depletion of 2DEG. According to the polarization theory,[3] the 2DEG density in the GaN layer is related to the polarization charge density, which changes with the thickness and the molar component of AlGaN.

Considering the large thickness of the GaN layer (d_2 equals 4 μm in this work), we think that the vertical electric field at the bottom of the GaN layer is zero. Thus, we have

$$\left.\frac{\partial \varphi_i(x,y)}{\partial y}\right|_{y=d_1+d_2} = 0, \quad i = 5,6,7,8. \quad (11)$$

The surface potential of the AlGaN layer below the gate electrode is equal to the voltage applied to the gate, with

$$\varphi_1(x,0) = V_{GS}. \quad (12)$$

According to the continuity of the interfacial potential in each region between AlGaN layer and GaN layer, we have

$$\varphi_1(x,d_1) = \varphi_5(x,d_1), \quad (13)$$

$$\varphi_2(x,d_1) = \varphi_6(x,d_1), \quad (14)$$

$$\varphi_3(x,d_1) = \varphi_7(x,d_1), \quad (15)$$

$$\varphi_4(x,d_1) = \varphi_8(x,d_1). \quad (16)$$

The applied bias voltage of the device satisfies the following formulas:

$$\varphi_1(0,d_1) = 0, \varphi_3(L_3,d_1) = V_{DS}. \quad (17)$$

According to the continuity of the potential and lateral electric field in region I–IV, we can obtain the following equations:

$$\begin{aligned}\varphi_1(L_1,d_1) &= \varphi_2(L_1,d_1) = V_1, \left.\frac{\partial \varphi_1(x,y)}{\partial x}\right|_{x=L_1,y=d_1} \\ &= \left.\frac{\partial \varphi_2(x,y)}{\partial x}\right|_{x=L_1,y=d_1}, \end{aligned} \quad (18)$$

$$\begin{aligned}\varphi_2(L_2,d_1) &= \varphi_3(L_2,d_1) = V_2, \left.\frac{\partial \varphi_2(x,y)}{\partial x}\right|_{x=L_2,y=d_1} \\ &= \left.\frac{\partial \varphi_3(x,y)}{\partial x}\right|_{x=L_2,y=d_1}, \end{aligned} \quad (19)$$

$$\begin{aligned}\varphi_3(L_3,d_1) &= \varphi_4(L_3,d_1) = V_3, \left.\frac{\partial \varphi_3(x,y)}{\partial x}\right|_{x=L_3,y=d_1} \\ &= \left.\frac{\partial \varphi_4(x,y)}{\partial x}\right|_{x=L_3,y=d_1}, \end{aligned} \quad (20)$$

where V_1, V_2, and V_3 represent the electric potential at the AlGaN/GaN heterojunction interface with $x = L_1$, L_2, and L_3, respectively, and their values can be determined by the continuity of the lateral electric field at the heterojunction interface from Eqs. (18)–(20).

For simplicity, in Eqs. (3)–(16) the device's built-in electric field is ignored because it is negligible compared with the device's applied voltage V_{DS}.

By applying Taylor's expansion to the potential distribution function along the y coordinate axis direction, we adopt the first three terms of the expression,[12] then we can acquire the expression of the potential distribution in region I–VIII as follows:

$$\begin{aligned}\varphi_i(x,y) &= \varphi_i(x,d_1) + \frac{\partial \varphi_i(x,d_1)}{\partial y}(y-d_1) \\ &+ \frac{\partial^2 \varphi_i(x,d_1)}{2\partial y^2}(y-d_1)^2, \\ &i = 1,2,3,4,5,6,7,8. \end{aligned} \quad (21)$$

Substituting Eq. (23) into Eqs. (1) and (2) and reducing the order of the Poisson's equation under the constraints of the boundary conditions, equations (3)–(16) lead to the expression of AlGaN/GaN interface potential distribution, ($i = 1,2,3,4$), which satisfies the differential equation as follows:

$$\frac{\partial^2 \varphi_1(x,d_1)}{\partial x^2} - \frac{\varphi_1(x,d_1)}{t_1^2} = \frac{-qN_1}{\varepsilon_1}, \quad (22)$$

$$\frac{\partial^2 \varphi_i(x,d_1)}{\partial x^2} - \frac{\varphi_i(x,d_1)}{t_i^2} = \frac{-qN_i x}{\varepsilon_1}, \quad i = 2,3,4, \quad (23)$$

$$t_1 = \left(\frac{\varepsilon_2 d_2 d_1}{\varepsilon_1} + \frac{d_1^2}{2}\right)^{1/2}, \quad (24)$$

$$t_i = \left(\frac{\varepsilon_2 d_2 d_3}{\varepsilon_3} + \frac{\varepsilon_1 d_1 d_3}{\varepsilon_3} + \frac{\varepsilon_2 d_1 d_2}{\varepsilon_1} + \frac{d_1^2}{2}\right)^{1/2}, \quad (25)$$

$$N_1 = \frac{d_1 N_{S1}}{t_1^2} + \frac{d_1^2 N_1}{2t_1^2} + \frac{d_2 d_1 N_2}{t_1^2} + \frac{V_{GS}\varepsilon_1}{t_1^2 q}, \quad (26)$$

$$\begin{aligned}N_i(x) &= \left(\frac{\varepsilon_1 d_3 + \varepsilon_3 d_1}{\varepsilon_3 t_i^2}\right) N_{Si} + \left[1 - \frac{\varepsilon_2 d_2}{\varepsilon_1}\left(\frac{\varepsilon_1 d_3 + \varepsilon_1 d_3}{\varepsilon_3 t_i^2}\right)\right] N_1 \\ &+ \left(\frac{\varepsilon_1 d_3 + \varepsilon_3 d_1}{\varepsilon_3 t_2^2} d_2\right) N_2 + \frac{Vp(x)\varepsilon_1}{t_i^2 q}. \end{aligned} \quad (27)$$

Using the above conditions, $\varphi_i(x,d_1)$ are obtained by solving Eqs. (22) and (23), which are given as

$$\varphi_1(x,d_1) = \frac{qN_1 t_1^2}{\varepsilon_1} + \left(V_1 - \frac{qN_1 t_1^2}{\varepsilon_1}\right)\frac{\sinh(x/t_1)}{\sinh(L_1/t_1)} - \left(\frac{qN_1 t_1^2}{\varepsilon_1}\right)\frac{\sinh((L_1-x)/t_1)}{\sinh(L_1/t_1)}, \quad 0 < L \le L_1, \quad (28)$$

$$\varphi_i(x,d_1) = \frac{qN_i,(x)t_i^2}{\varepsilon_1} + \left(V_i - \frac{qN_{i2}t_i^2}{\varepsilon_1}\right)\frac{\sinh((x-L_{i-1})/t_i)}{\sinh((L_i-L_{i-1})/t_i)} + \left(V_{i-1} - \frac{qN_{i1}t_i^2}{\varepsilon_1}\right)\frac{\sinh((L_i-x)/t_i)}{\sinh((L_i-L_{i-1})/t_i)}, \quad L_{i-1} < x \le L_i, \quad i = 2,3,4. \tag{29}$$

The lateral electric field distribution along the channel are now readily obtained from Eqs. (25) and (26) as:

$$E_1(x,d_1) = \frac{\partial\varphi_1(x,d_1)}{\partial x} = \left(V_1 - \frac{qN_1t_1^2}{\varepsilon_1}\right)\frac{\cosh(x/t_1)}{t_1\sinh(L_1/t_1)} + \left(\frac{qN_1t_1^2}{\varepsilon_1}\right)\frac{\cosh((L_1-x)/t_1)}{t_1\sinh(L_1/t_1)}, \quad 0 < x \le L_1, \tag{30}$$

$$E_i(x,d_1) = k_i + \left(V_i - \frac{qN_{i2}t_i^2}{\varepsilon_1}\right)\frac{\cosh((x-L_{i-1})/t_i)}{t_2\sinh((L_i-L_{i-1})/t_i)} - \left(V_{i-1} - \frac{qN_{i1}t_i^2}{\varepsilon_1}\right)\frac{\cosh((L_i-x)/t_i)}{t_2\sinh((L_i-L_{i-1})/t_i)}, \quad L_{i-1} < x \le L_i, \quad i = 2,3,4. \tag{31}$$

With $N_{i1} = N_i(L_{i-1})$, $N_{i2} = N_i(L_i)$. k_i donates the slope of $V_p(x)$ at L_i, $i = 2, 3, 4$.

3. Results and discussion

According to the above analysis, from Fig. 2 we can see the potential distributions along the channel for different charge doping densities when l_1 and l_2 are fixed, where the dotted lines represent the numerical results of the analytical model and the solid lines with symbol denote the simulation results obtained from the ISE TCAD software.

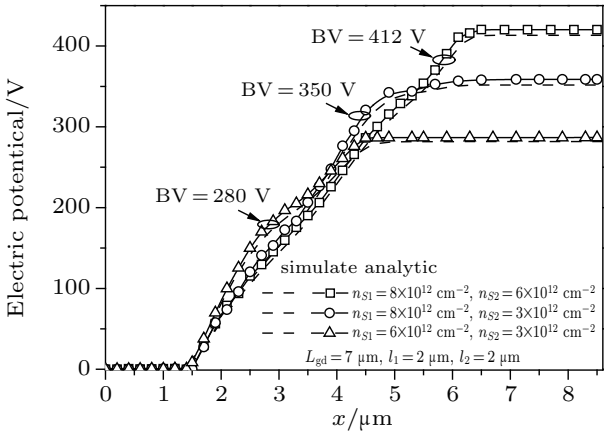


Fig. 2. Potential distributions for various charge doping densities.

We can see from Fig. 3 that the simulation results of the potential are in good agreement with the numerical results, Moreover, we can observe that with the increase of the total charge quantity of two doping regions, the increasing speed of the channel potential becomes faster, which means that a higher electric field appears. It is bad for improving the breakdown voltage. The dependence of channel electric field on n_{S1} and n_{S2} at $l_1 = l_2 = 2$ μm are illustrated in Fig. 3. We can see clearly that there is a new electric field peak in the doping region close to the gate edge. Besides, the electric field peak below the gate is reduced by 28% when n_{S2} is increased from 3×10^{12} cm^{-2} to 6×10^{12} cm^{-2}, with n_{S1} kept the same. Furthermore, another effect can be observed, i.e. a significant new electric field peak also appears at the boundary of the region near the drain edge. That is due to the fact that the 2DEG is fully depleted. Therefore, it is very important to increase the overall charge doping density appropriately in order to improve the breakdown voltage.

From Figs. 4 and 5, we can see the variations of the channel potential and the lateral electric field with the negative charge doping length l_1 and l_2 when the negative charge doping densities n_{S1} and n_{S2} are fixed, respectively. In Fig. 4, we can observe that as the total charge doping length $l_1 + l_2$ increases, the channel potential grows slower, which indicates the channel electric field becomes smaller and the electric field distribution is more even. Combining the results shown in Fig. 5, we can see from similar results shown in Fig. 5 that there appear new obvious electric field peaks. What is more, the positions of electric field peaks are closely related to the negative charge doping position. For example, when the total doping length increases from 2 μm to 4 μm, there is another new electric field peak arising in the doping region near the drain edge. Moreover, when the total doping length increases from 4 μm to 5 μm, we can observe the second electric field peak that shifts to the drain edge. The results we see can be attributed to the fact that more 2DEGs are depleted in the channel with $l_1 + l_2$ increasing, and the electric field modulation effect caused by the difference between charge doping densities in two regions. Thus, a higher drain bias voltage can be applied to the RESURF AlGaN/GaN HEMTs.

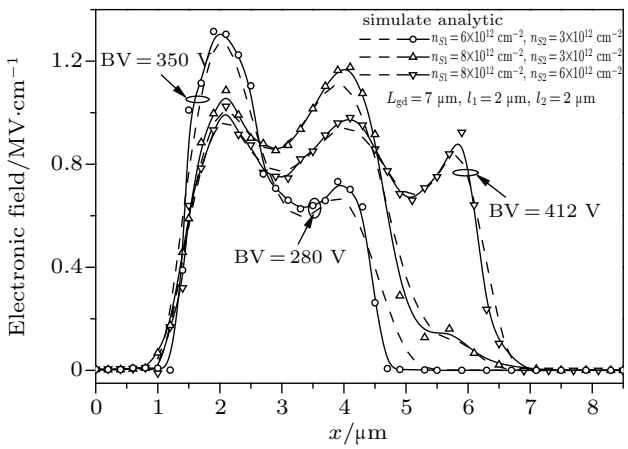


Fig. 3. Lateral electric fields for various charge doping densities.

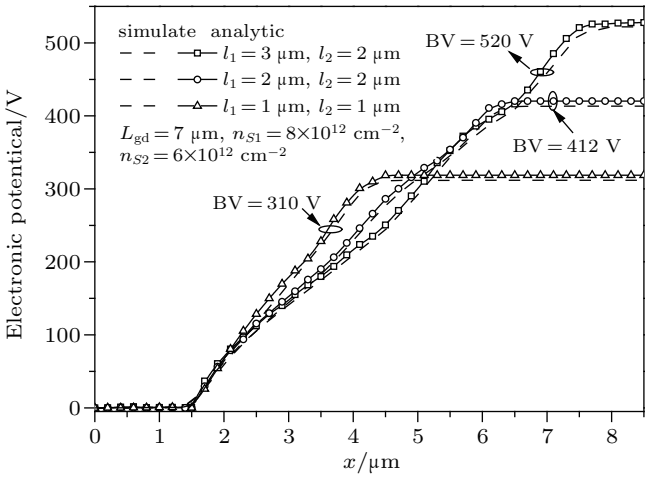


Fig. 4. Potential distributions for various charge doping positions.

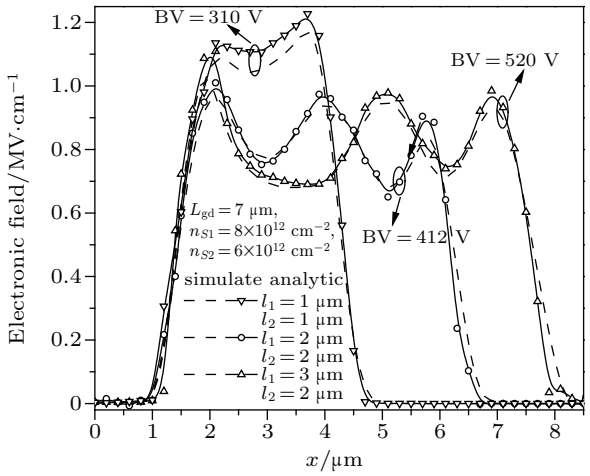


Fig. 5. Lateral electric fields for various charge doping positions.

4. Conclusions

In this paper, an analytical model for the channel potential and electric field distributions of the RESURF AlGaN/GaN HEMTs is presented. It is derived as a function of device parameters. The analytic results from the derived expression are in good agreement with the simulated results generated from ISE. This demonstrates the validity of the analytical model. The analytical results from the given expression accord fairly with the simulation results obtained from ISE, demonstrating the validity of the model. The dependence of lateral electric field and potential distribution on negative charge doping density and doping length are discussed, respectively. We find that with negative charge doping length fixed, as the doping density increases, the channel potential grows slower, the electric field peak below the gate decreases, and new electric field peaks at the boundary of doping region in RESURF AlGaN/GaN HEMT appear. Conversely, we can see a similar phenomenon when negative charge doping densities of two doping regions are the same and charge doping length is varying. The model can be a powerful tool for device designers to optimize the device structure and have a physical insight into the RESURF AlGaN/GaN HEMTs.

References

[1] Cai Y, Zhou Y, Chen K J and Lau K M 2005 *IEEE Electron. Dev. Lett.* **26** 435

[2] Saito W, Takada Y, Kuraguchi M, Tsuda. K, Omura I, Ogura T and Ohashi H 2003 *IEEE Trans. Electron. Dev.* **50** 2528

[3] Ambacher O, Foutz B, Smart J, Shealy J R, Weimann N G, Chu K, Murphy M, Sierakowski A J, Schaff W J and EastmanFoutz L F 2000 *J. Appl. Phys.* **87** 334

[4] Ambacher O, Dimitrov R, Stutzmann M, Foutz B E, Murphy M J, Smart J A, Shealy J R, Weimann N G, Chu K, Chumbes M, Green B, Sierakowski A J, Schaff W J and Eastman L F 1999 *Phys. Status Solidi* **216** 381

[5] Asbeck P M, Yu E T and Lau S S 1997 *Electron. Lett.* **33** 1230

[6] Ludikhuize A W 2002 *12th Int. Symp. Power Semicond. Dev. & Ics. Proc.*, 22–25 May, 2000, Toulouse, France, p. 11

[7] Duan B X and Yang Y T 2012 *Sci. China: Inform. Sci.* **42** 770

[8] Zhao Z, Luo Q and Du J 2013 *Electron. Lett.* **49** 1638

[9] Mao W, She W B, Yang C, Zhang C, Zhang J C, Ma X H , Zhang J F, Liu H X, Yang L A, Zhang K, Zhao S L, Chen Y H, Zheng X F and Hao Y 2014 *Chin. Phys. B* **23** 087305

[10] Kumar S P, Agrawal A, Chaujar R, Gupta M and Gupta R S 2008 *Superlattices & Microstruct.* **44** 37

[11] Duan B X, Yang Y and Zhang B 2010 *Solid State Electron.* **54** 685

[12] Ahmed T, Khan M T A, Islam M S 2012 *International Conference on Devices, Circuits and Systems (ICDCS)*, March 15–16, Coimbatore, India, p. 226